



ORIGINAL ARTICLE

OPEN

Single-cell analyses unravel ecosystem dynamics and intercellular crosstalk during gallbladder cancer malignant transformation

Zhaobin He^{1,2}  | Jianqiang Cao^{1,2} | Xiqiang Wang^{1,2} | Shengbiao Yang^{1,2} |
 Huijie Gao^{1,2} | Yongzhe Yu³ | Zequn Di^{2,4} | Cheng Peng^{1,2} 

¹Department of Hepatobiliary Surgery, Qilu Hospital, Shandong University, Jinan, Shandong Province, China

²Department of Hepatobiliary Minimally Invasive Surgery, Shandong University Institute of Endoscopic Minimally Invasive Surgery, Jinan, Shandong Province, China

³Department of Geriatric Medicine, Qilu Hospital of Shandong University, Jinan, Shandong Province, China

⁴Department of Clinical Medicine, School of Basic Medical Sciences Nanchang University, Nanchang, Jiangxi Province, China

Correspondence

Cheng Peng, Department of Hepatobiliary Surgery, Qilu Hospital, Shandong University, Jinan, Shandong Province 250012, China.
 Email: Dr.Peng@email.sdu.edu.cn

Abstract

Background: Gallbladder cancer (GBC) is a rare but aggressive malignancy, often detected late due to early asymptomatic stages. Understanding cellular and molecular changes from normal tissue to high-grade intraepithelial neoplasia (HGIN) and invasive GBC is vital for identifying early biomarkers and therapeutic targets.

Methods: We performed single-cell RNA sequencing on 98,113 cells derived from 2 normal adjacent tissues (NAT), 2 HGIN, and 6 GBC samples. The cellular diversity and heterogeneity, particularly within epithelial and immune cell populations in NAT–HGIN–GBC, were investigated utilizing single-cell RNA sequencing, bulk RNA sequencing (bulk RNA-seq), and 10 machine learning methodologies. Furthermore, the intercellular crosstalk between epithelial cells and tumor immune microenvironment cells was examined and validated through multiplex immunofluorescence staining.

Results: The constructed cell atlas elucidated alterations in the immune landscape across various states of NAT–HGIN–GBC, highlighting a more pronounced inhibitory immune microenvironment in GBC. The epithelial subtype TOP2A+ Epi is markedly elevated in GBC and is correlated with a poor prognosis. Key genes associated with this subtype may include GMNN, CYTOR, KLK6, and BIRC5. Similarly, immunosuppressive macrophages, identified as TOP2A+ Macro, also increase along the NAT–HGIN–GBC sequence and are linked to reduced patient survival. Furthermore, TOP2A+

Abbreviations: CD163, macrophage marker; CD3D, CD3E, T cell markers; CD68, macrophage marker; CNV, copy number variation; COL1A1, collagen type I alpha 1 chain; CSF3R, receptor for granulocyte colony-stimulating factor; DEGs, differentially expressed genes; EPCAM, epithelial cell adhesion molecule; FN14, fibroblast growth factor-inducible 14; GBC, gallbladder cancer; GNLY, granulysin; GSEA, gene set enrichment analysis; HGIN, high-grade intraepithelial neoplasia; Hippo, A pathway regulating cell growth; KRT19, Keratin 19; MAPK, mitogen-activated protein kinase; ML, machine learning; MS4A1, marker of B cells; NAT, normal adjacent tissue; NKG7, natural killer cell marker; PD-1, programmed cell death protein 1; PD-L1, programmed death-ligand 1; PECAM1, platelet endothelial cell adhesion molecule 1; scRNA-seq, single-cell RNA sequencing; TAMs, tumor-associated macrophages; TIGIT, T cell immunoreceptor with Ig and ITIM domains; TIME, tumor immune microenvironment; TME, tumor microenvironment; TPSAB1, mast cell marker; TWEAK, TNF-like weak inducer of apoptosis; Wnt, wingless-related integration site signaling.

Supplemental Digital Content is available for this article. Direct URL citations are provided in the HTML and PDF versions of this article on the journal's website, www.hepcommjournal.com.

This is an open access article distributed under the terms of the Creative Commons Attribution-Non Commercial-No Derivatives License 4.0 (<http://creativecommons.org/licenses/by-nc-nd/4.0/>), where it is permissible to download and share the work provided it is properly cited. The work cannot be changed in any way or used commercially without permission from the journal.

Copyright © 2025 The Author(s). Published by Wolters Kluwer Health, Inc. on behalf of the American Association for the Study of Liver Diseases.

Macro and CD8⁺ exhausted T cells (CD8⁺ Tex) engage in intercellular communication with epithelial TOP2A+Epi cells via the TWEAK/FN14 signaling pathway, thereby promoting tumor progression and immune evasion in GBC. The findings were further corroborated through multiplex immunofluorescence staining conducted on specimens from patients.

Conclusions: This study elucidates significant alteration in the cellular ecosystems and intercellular signaling within the tumor immune microenvironment across the NAT–HGIN–GBC sequence. It identifies TOP2A, TWEAK, and FN14 as potential biomarkers and therapeutic targets for GBC.

Keywords: intercellular communication, single-cell RNA sequencing, TOP2A, tumor immune microenvironment, TWEAK/FN14 signaling

INTRODUCTION

Gallbladder cancer (GBC) is an uncommon yet highly aggressive malignancy within the biliary tract cancers.^[1] Despite its low incidence, GBC poses significant challenges due to its asymptomatic nature in early stages and its rapid progression, often resulting in late diagnosis and a 5-year survival rate of <20%.^[2] GBC develops through 2 distinct primary pathways. The more prevalent pathway is linked to cholecystitis induced by cholelithiasis, predominantly affecting elderly individuals, particularly women.^[3] The second pathway, associated with anomalous pancreaticobiliary duct junction (APBDJ), predominantly occurs in young patients in Japan, exhibiting less female predominance and lower rates of cholelithiasis.^[4,5] At the molecular level, GBC related to APBDJ frequently involves mutations in KRAS followed by TP53, whereas GBC-associated cholelithiasis typically presents with early TP53 mutations and infrequent KRAS involvement. This distinction suggests the need for tailored diagnostic approaches.^[6,7] However, both pathways converge during their progression through high-grade intraepithelial neoplasia (HGIN), also referred to as severe dysplasia, and carcinoma in situ, ultimately culminating in invasive carcinoma.^[8,9] At present, research on the mechanisms driving the transition from HGIN to GBC remains insufficient.

The tumor immune microenvironment (TIME) is pivotal in cancer progression, as it modulates immune responses and fosters an immunosuppressive milieu that facilitates tumor growth, invasion, and metastasis.^[10] The majority of GBCs are characterized by an immune-suppressed microenvironment, which results in a low objective response rate to immune checkpoint inhibitor therapy.^[11] Single-cell RNA sequencing (scRNA-seq) has markedly enhanced our comprehension of the TIME by facilitating high-resolution characterization of the diverse immune cell populations and their functional states within tumors. This technology elucidates the

intercellular interactions that drive cancer progression and informs the development of more effective cancer immunotherapies.^[12] However, the rarity of GBC and the challenges associated with obtaining fresh tissue samples substantially impede comprehensive single-cell analysis studies of this malignancy.^[13] Zhang et al demonstrated that elevated levels of midkine (MDK) in GBC interact with its receptor, LDL receptor-related protein 1 (LRP1), to facilitate the differentiation of immunosuppressive macrophages. Furthermore, they found that CXCL10 secreted by macrophages, and its receptor CXCR3 engage in crosstalk with regulatory T cells (Tregs) in GBC cases exhibiting ErbB pathway mutations.^[14] Wang et al^[15] identified distinct cellular reprogramming events in GBC, transitioning from inflammation to malignancy, and pinpointed key markers for early-stage carcinogenesis as well as potential therapeutic targets. Xie et al^[16] explored immune alterations in GBC liver metastasis following PD-1 blockade, underscoring potential biomarkers for predicting immunotherapy outcomes. Chen et al^[17] employed scRNA-seq to analyze samples from 5 patients, including primary tumors, lymph node metastases, and adjacent normal tissues, to investigate cellular heterogeneity and microenvironmental dynamics in GBC. In a separate study, He et al utilized both scRNA-seq and whole-genome sequencing on a variety of gallbladder disease samples to uncover a suppressive immune microenvironment in GBC. They identified OLFM4 as a critical factor driving GBC progression by promoting immune evasion through mechanisms such as T-cell dysfunction, macrophage infiltration, and PD-L1 expression via the MAPK–AP1 signaling axis.^[18]

Despite significant advancements in the understanding of GBC and its immune microenvironment, the progression from normal adjacent tissue (NAT) through HGIN to invasive GBC remains insufficiently explored. This transformation entails critical alterations in cellular composition and immune modulation, which are

essential to understanding GBC pathogenesis. This study seeks to address this research gap by using scRNA-seq to analyze the dynamic changes across the NAT–HGIN–GBC sequence. By revealing shifts within the TIME and identifying key regulatory pathways and intercellular ligand–receptor interactions, our research aims to uncover potential biomarkers and therapeutic targets critical for early intervention and improved management of GBC.

METHODS

Patient enrollment and specimen collection

A total of 10 surgically resected fresh tissue samples were collected, including 2 NAT (P1, P3), 2 HGIN (P2, P4), and 6 GBC (P1, P3, P5–P8), from patients who had not received any prior treatment, between November 2023 and March 2024. Detailed information on patient characteristics and sample types is provided in Supplemental Table S1, <http://links.lww.com/HC9/B963>. Written informed consent was obtained from each patient, and the study was approved by the Institutional Review Board of Qilu Hospital (registration number: KYLL-2024 (ZM)-685).

Single-cell capture and cDNA synthesis

Single-cell capture and cDNA synthesis were performed using the Single Cell 3' Library and Gel Bead Kit V3.1 (10× Genomics, 1000121) and the Chromium Single Cell G Chip Kit (10× Genomics, 1000120). The cell suspension, containing 300–600 viable cells per microliter as determined by Count Star, was loaded onto the Chromium Single Cell Controller (10× Genomics) to produce single-cell gel beads in emulsion (GEMs) according to the manufacturer's protocol. Briefly, single cells were suspended in PBS with 0.04% bovine serum albumin, and ~6000 cells were added per channel, aiming to recover around 3000 cells. Captured cells were lysed, and RNA was released and barcoded through reverse transcription within individual GEMs. Reverse transcription was performed using an S1000TM Touch Thermal Cycler (Bio-Rad) at 53°C for 45 minutes, followed by 85°C for 5 minutes, and held at 4°C. The cDNA was then generated and amplified, and its quality was assessed using an Agilent 4200 system (performed by CapitalBio Technology).

scRNA-seq library preparation

Single-cell RNA-seq libraries were constructed using the Single Cell 3' Library and Gel Bead Kit

V3.1 according to the manufacturer's instructions. Sequencing was performed on an Illumina NovaSeq. 6000 sequencer, achieving a sequencing depth of at least 100,000 reads per cell with a paired-end 150 bp (PE150) strategy (performed by CapitalBio Technology).

scRNA-seq data processing

Raw gene expression matrices for each sample were generated using the Cell Ranger pipeline with the human reference genome version GRCh38.

The filtered gene expression matrices were analyzed using R software with the Seurat package. In brief, genes expressed in more than 0.1% of cells and cells with over 200 detected genes were selected for further analysis. Low-quality cells were excluded if they met the following criteria: (1) fewer than 200 genes detected or (2) >20% of UMIs (unique molecular identifiers) derived from mitochondrial genes. After filtering, the gene expression matrices were normalized using the `NormalizeData` function, and 2000 highly variable features were identified using the `FindVariableFeatures` function. Principal component analysis (PCA) was performed on scaled data using the `RunPCA` function with default settings to reduce dataset dimensionality. The `ElbowPlot` and `DimHeatmap` functions were used to determine the appropriate dimensionality for each dataset. Cell clustering was conducted using the `FindNeighbors` function (top 15 principal components) and the `FindClusters` function (resolution=0.5), followed by nonlinear dimensional reduction using the `RunUMAP` function with default parameters. Differentially expressed genes (DEGs) for each cluster were identified using the Wilcoxon test. Genes with significant differences in expression (adjusted p value <0.05 and log FC >0.25) were considered marker genes. Clusters were annotated based on these marker genes to determine specific cell types. For each major cell type, sub-clustering was performed by extracting the relevant cells from the integrated dataset and conducting clustering again using cell-type-specific resolution.

Gene set enrichment analysis

Gene set enrichment analysis (GSEA) was performed to identify enriched biological processes and pathways associated with the DEGs in each cluster. The DEGs from each cluster were ranked by log fold change, and GSEA was conducted using the `clusterProfiler` package in R. We used the Molecular Signatures Database (MSigDB) for pathway annotations, focusing on hallmark gene sets (H) and Gene Ontology (GO) terms.

Enrichment scores and significance levels were calculated to determine the pathways that were significantly associated with each cluster. Pathways with an adjusted p value < 0.05 were considered significantly enriched. Visualization of enriched pathways was carried out using the *enrichplot* and *ggplot2* packages in R to generate dot plots and enrichment plots, highlighting key biological processes involved in the different cell populations.

Single-cell trajectories analysis

Single-cell trajectories were constructed using the *monocle 2* R package, introducing the concept of pseudotime to infer cell developmental progressions. Genes were filtered based on the following criteria: expressed in more than 10 cells, average expression greater than 0.1, and a Q value below 0.01 across different analyses.

CytoTRACE analysis

To estimate the differentiation potential of cells, we employed the CytoTRACE algorithm, which predicts differentiation states based on gene expression profiles.^[19] This analysis served as a validation of the trajectory analysis, offering an independent perspective on cellular differentiation.

Copy number variations analysis

We used the *InferCNV* R package to analyze copy number variation (CNV) across epithelial cells in different groups. CNVs were estimated by comparing gene expression levels against a reference set of NAT epithelial cells. The analysis was performed using default parameters, including a window size of 101 genes and a smoothing function to reduce noise in the data. To distinguish malignant cells, we established baselines for nonmalignant epithelial clusters by analyzing moving-averaged expression profiles with a 100-gene sliding window. Cells were quantified through CNV scores (genome-wide mean squared values) and Pearson correlation with malignant cell CNV profiles.^[20]

Bulk RNA-seq datasets analysis

We obtained 2 public cholangiocarcinoma datasets from the Gene Expression Omnibus (GEO) and The Cancer Genome Atlas (TCGA), specifically GSE244807 and TCGA-CHOL. Data from both datasets were preprocessed, normalized, and log-transformed to ensure consistency.

Cell-type deconvolution of GEO samples

Cell-type deconvolution of GEO samples (GSE244807) was performed to estimate the proportions of different cell types in the bulk RNA-seq data. We used the *BayesPrism* R package to deconvolute the bulk expression profiles into cell type-specific proportions, leveraging the scRNA-seq data as a reference.

Machine learning analysis with Mime

We used the *Mime* R package to identify key prognostic features, a versatile machine-learning framework for building and visualizing predictive models.^[21] *Mime* integrates various machine learning algorithms to simplify model construction and feature selection, enabling effective use of complex transcriptomic datasets. We applied the package to create prognostic models based on RNA-seq data from our study, aiming to identify gene signatures linked to patient outcomes. Models were built using cross-validation, and their performance was assessed with metrics such as the concordance index (C-index) and the area under the receiver operating characteristic (AUC) curve.

Cell-cell communication analysis with CellChat

The *CellChat* R package was utilized to investigate ligand–receptor interactions between epithelial and TIME cells, as outlined in a previous study.^[22] Receptors and ligands expressed in over 10% of cells within a specific cluster were selected for subsequent analysis. The putative ligand–receptor pairs were visualized using the *ggplot2* package to illustrate interactions between distinct cell subpopulations.

Multiplex immunofluorescence staining

Paraffin-embedded tissue sections were dewaxed, rehydrated, and subjected to antigen retrieval in pH 6.0 citrate buffer. Endogenous peroxidase activity was blocked using 3% hydrogen peroxide, followed by serum blocking with 10% rabbit serum or 3% bovine serum albumin, depending on the primary antibody source. Sequential primary antibody incubations were performed at 4 °C overnight, each followed by incubation with species-specific HRP-conjugated secondary antibodies and tyramide signal amplification for fluorescence detection. After each tyramide signal amplification application, slides underwent microwave treatment in citrate buffer to remove the primary and secondary antibodies, allowing for sequential rounds of staining. This cycle was repeated for each marker, including TWEAK, FN14,

TOP2A, and CD68. Finally, sections were counterstained with DAPI, quenched for autofluorescence, and mounted with an antifade mounting medium. Images were acquired with a high-resolution fluorescence microscope, and co-localization and spatial relationships of markers were analyzed digitally.

Statistical analysis

All statistical analyses were conducted using R language (version 4.2.2) software. Kaplan–Meier survival analysis was performed using the R packages “survminer” and “survival.” Specifics regarding statistical tools, methods, and significance thresholds are provided in the relevant methods, results sections, and figure legends.

RESULTS

Altered subpopulation patterns of cells in the NAT–HGIN–GBC progression

We collected a total of 10 samples, including 2 NAT, 2 HGIN, and 6 GBC, to investigate tumor heterogeneity, cellular diversity, and molecular characteristics along the NAT–HGIN–GBC progression (Figure 1A). Following rigorous quality control measures, we analyzed 98,113 cells and identified 10 distinct cell types using canonical marker genes. These included epithelial cells (EPCAM and KRT19), T and NK cells (CD3D, CD3E, NKG7, and GNLY), B cells (MS4A1 and CD79A), plasma B cells (IGHG1), neutrophils (CSF3R), macrophages (CD163 and CD68), mast cells (TPSAB1), fibroblasts (COL1A1 and ACTA2), stromal cell (IGHG1 and COL1A1), and endothelial cells (PECAM1 and KRT19) (Figures 1B–E and Supplemental Figures S1A, B, <http://links.lww.com/HC9/B964>). The DEGs and marker genes corroborated the precision cell type identification (Figure 1F and Supplemental Figure S1C, <http://links.lww.com/HC9/B964>). Notably, the populations of epithelial, macrophage, and neutrophil cells were more abundant in tumor samples (HGIN and GBC), compared to benign controls (NAT). Conversely, the populations of T, NK, and B cells were more prominent in the control sample than in the tumor samples (Figure 1G and Supplemental Figure S1D, <http://links.lww.com/HC9/B964>). These observations indicate an increased malignancy in GBC, characterized by a predominantly immunosuppressive tumor microenvironment (TME).

Elevation of TOP2A+Epithelial drives the NAT–HGIN–GBC progression

Initially, we analyzed chromosomal CNVs across all epithelial cells, revealing a progressive increase in CNV

levels along the NAT–HGIN–GBC progression, which reflects heightened genomic instability as cancer progresses. Notably, epithelial cells from GBC showed significantly more chromosomal amplifications and deletions compared to those from NAT and HGIN (Figure 2A). To further elucidate the heterogeneity of epithelial cells, we performed an in-depth analysis of epithelial subtypes. A total of 21,629 epithelial cells were re-clustered into 6 distinct subpopulations (Epi0–Epi5), each characterized by specific individual markers, including MUC16+Epi (Epi0), TM4SF4+Epi (Epi1), SRGN+Epi (Epi2), TOP2A+Epi (Epi3), FGF3+Epi (Epi4), and KRT6A+Epi (Epi5). FGF3+Epi and KRT6A+Epi cells represent cancer-associated epithelial cells that are uniquely present in GBC (Figure 2B and Supplemental Figures S2A–C, <http://links.lww.com/HC9/B964>). Based on CNV scores and correlation analyses, we extracted malignant epithelial cells and performed a re-clustering. Our findings revealed that, in addition to the cancer-associated epithelial subtypes FGF3+Epi and KRT6A+Epi, the TOP2A+Epi subgroup exhibited the highest proportion of malignant cells (Figure 2C and Supplemental Figures S2D, E, <http://links.lww.com/HC9/B964>). Our analysis revealed that the proportions of MUC16+Epi and TOP2A+Epi cells, compared to other clusters, consistently increased across the NAT–HGIN–GBC sequence, with the TOP2A+ subtype showing a more dramatic elevation specifically in GBC (Figure 2D and Figure S2F, G, <http://links.lww.com/HC9/B964>). These observations suggest that these subtypes may play a significant role in facilitating tumor progression and malignancy in GBC.

We further performed GSEA and discovered that distinct epithelial clusters and groups demonstrated unique biological functions. The GBC group showed significant engagement in various tumor-associated signaling pathways, including Wnt, Hippo, and MAPK, as well as pathways related to protein synthesis and metabolism, such as Ribosome, Spliceosome, and Proteasome. Conversely, the NAT and HGIN groups were primarily enriched in immune-related pathways, indicating a more immunologically active TME in comparison to the GBC group. In particular, the TOP2A+ Epi subtype within the tumor cohort exhibited enrichment in DNA replication and cell cycle pathways, underscoring its potential role in facilitating accelerated cell proliferation and tumor progression (Figure 2E). To elucidate the underlying evolution of cellular states among epithelial cells, we employed trajectory analysis using the Monocle 2 algorithm. The resultant inferred state transition trajectory delineated 2 distinct lineages, manifesting a bifurcated structure transitioning from a progenitor state to a terminal differentiation state. By integrating insights from clustering and pseudotime analyses, TOP2A+ and MUC16+ Epi epithelial cells were found to occupy intermediate to late differentiation states (Figure 2F and Supplemental Figure S2H, <http://links.lww.com/HC9/B964>).

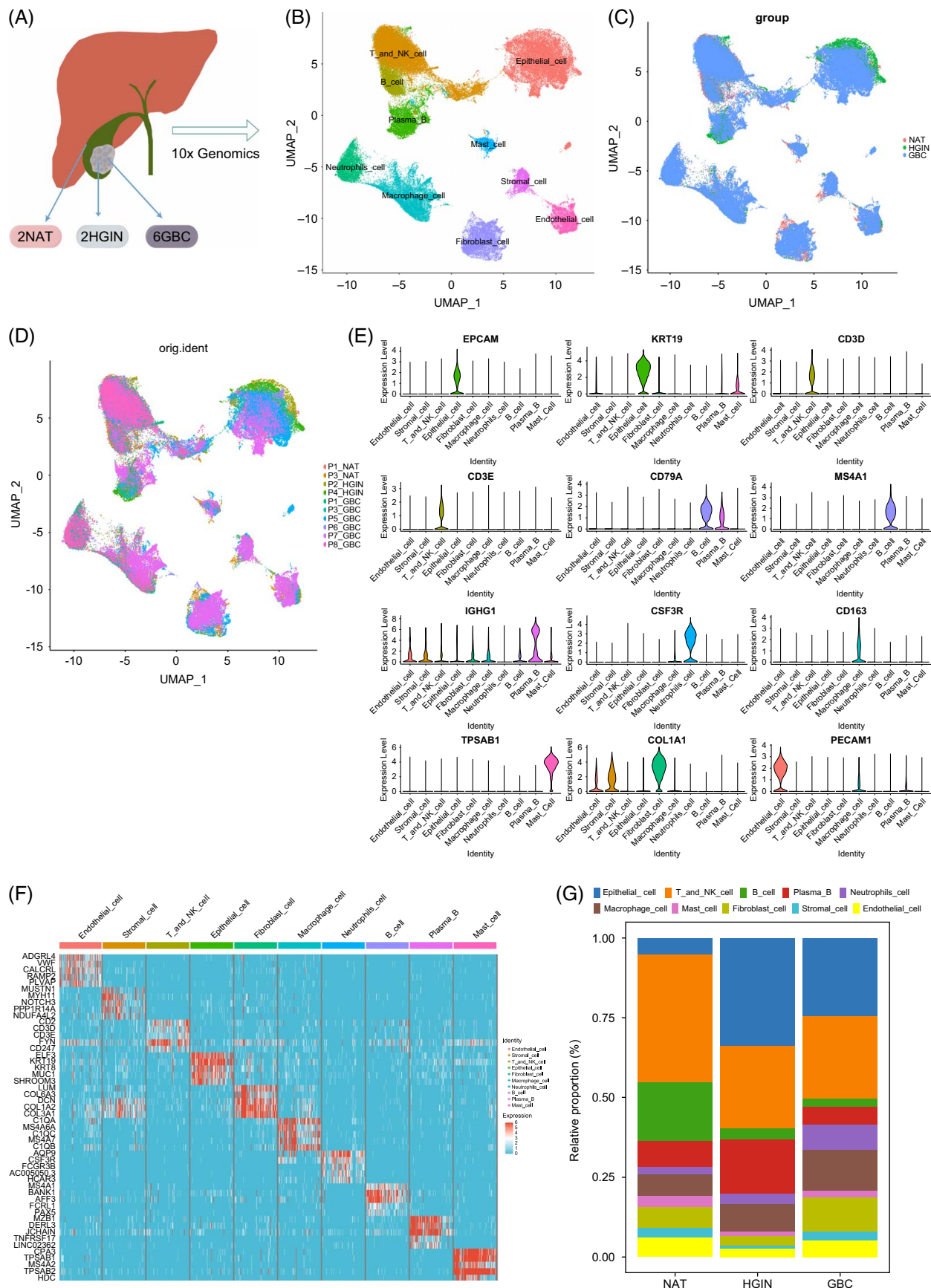


FIGURE 1 scRNA-seq analysis of cellular heterogeneity across NAT, HGIN, and GBC samples. (A) Schematic showing sample collection and analysis workflow. (B) UMAP clustering of cells with color-coded cell types. (C) UMAP plot of cells color-coded by sample group (NAT, HGIN, and GBC). (D) UMAP plot of cells color-coded by individual sample origin. (E) Violin plots showing canonical marker gene expression levels across identified cell types. (F) Heatmap depicting differentially expressed genes across cell clusters. (G) Stacked bar plot showing the relative proportions of each cell type in NAT, HGIN, and GBC samples. Abbreviations: GBC, gallbladder cancer; HGIN, high-grade intraepithelial neoplasia; NAT, normal adjacent tissue; scRNA-seq, single-cell RNA sequencing; UMAP, uniform manifold approximation and projection.

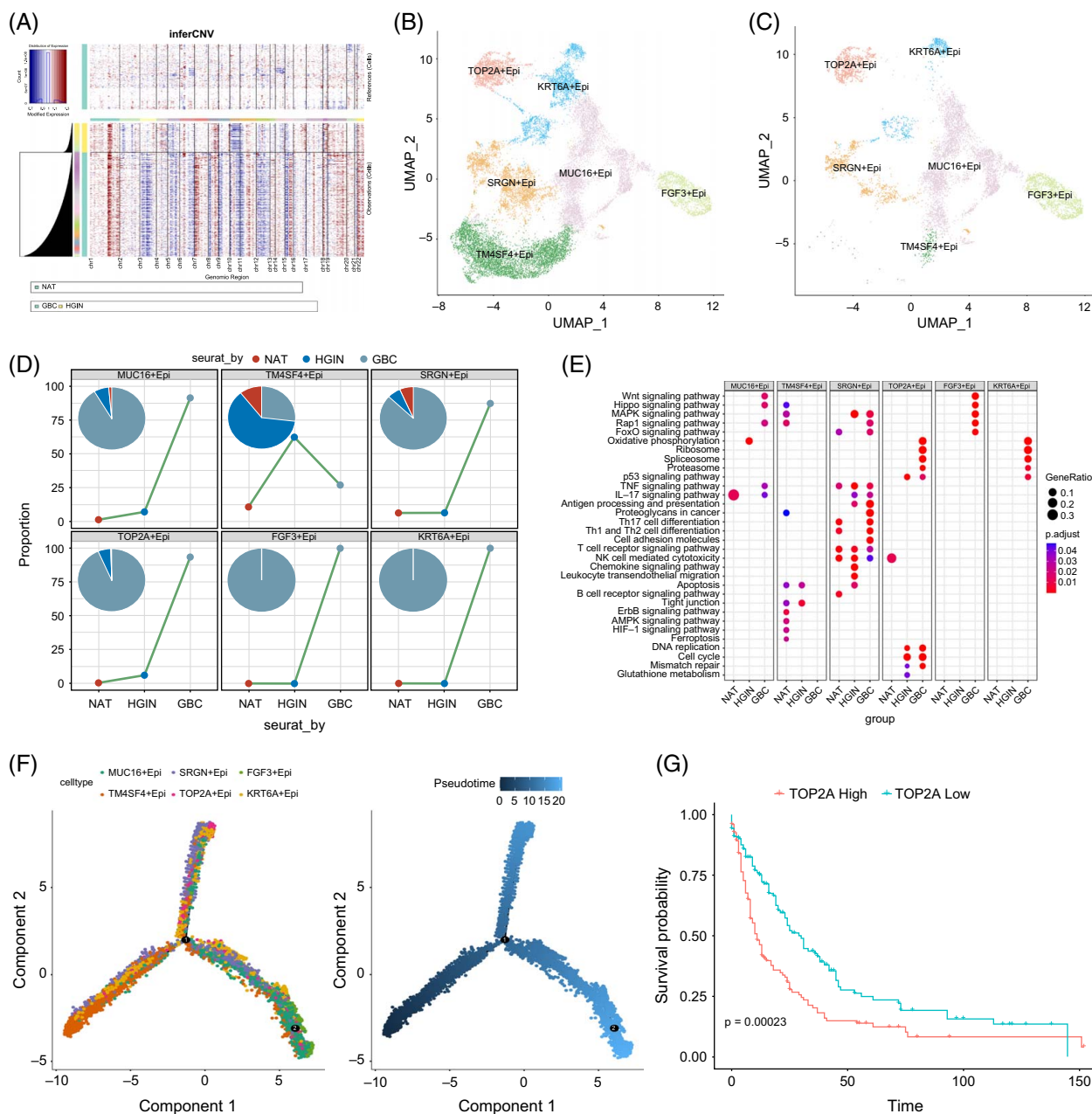


FIGURE 2 Analysis of epithelial cell subtypes. (A) InferCNV analysis showing inferred CNVs across epithelial cells from NAT, HGIN, and GBC samples. Blue and red colors represent deletions and amplifications, respectively, with increased CNV levels observed in GBC compared to NAT and HGIN. (B) UMAP clustering of epithelial cells identifying specific subtypes. (C) UMAP clustering of malignant epithelial cells identified based on CNV analysis. (D) Pie and line plots comparing the proportions of each epithelial subtype across different groups. (E) Dot plot showing enriched signaling pathways and biological processes in each epithelial subtype. (F) Pseudotime trajectory analysis of epithelial cells, showing differentiation pathways with color-coded cell types (left) and pseudotime progression (right). (G) Kaplan-Meier survival curves for patients stratified by the presence of TOP2A+ Epi subtype show worse survival outcomes for patients with a higher proportion of TOP2A+ Epi cells ($p = 0.0023$). Abbreviations: CNV, copy number variation; Epi, epithelial cell; GBC, gallbladder cancer; HGIN, high-grade intraepithelial neoplasia; NAT, normal adjacent tissue; UMAP, uniform manifold approximation and projection.

links.lww.com/HC9/B964). CytoTRACE scores were calculated for each epithelial cell, revealing that TOP2A+ and MUC16+ Epi cells were in intermediate differentiation states, whereas FGF3+ Epi and KRT6A+ Epi cells were in late differentiation states (Supplemental Figure S2I, <http://links.lww.com/HC9/B964>). These results imply that these subpopulations may be instrumental in promoting tumor aggressiveness and establishing terminally differentiated cancer phenotypes. Furthermore, cell-type deconvolution using the BayesPrism R package on RNA-seq data from the GSE244807 cohort demonstrated an association between the TOP2A+ Epi subtype and poor patient survival (Figure 2G). In summary, the findings suggest that the TOP2A+ Epi subtype is instrumental in advancing the progression of the NAT–HGIN–GBC sequence.

To pinpoint key genes linked to TOP2A+ Epi, we identified the top 300 DEGs from the TOP2A+ Epi subtypes as potential candidates. For this purpose, we employed the GSE244807 dataset for training and the TCGA-CHOL cohort for validation. Using the Mime R package, we developed 117 models by integrating ten distinct machine learning algorithms. Among the evaluated models, the combined RSF + StepCox[both] exhibited the highest mean C-index in both the training and validation cohorts, with values of 0.71 and 0.61, respectively, thereby indicating its superior performance (Figure 3A). By employing the median risk score derived from this selected model, we stratified patients into high-risk and low-risk groups. Notably, patients classified within the high-risk group exhibited significantly poorer outcomes in the GSE244807 cohort (Figure 3B). The discriminatory efficacy of the model was assessed using ROC analysis, yielding AUC values of 0.820, 0.817, and 0.766 for the 1-year, 3-year, and 5-year outcomes in the GSE244807 cohort, and 0.697, 0.638, and 0.582 for the TCGA-CHOL cohort, respectively (Figure 3C and Supplemental Figures S3A–F, <http://links.lww.com/HC9/B964>). Additionally, we identified the top 20 core genes associated with prognosis, including GMNN, CYTOR, KLK6, and BIRC5 (Figures 3D–F). These genes were found to play pivotal roles in cell cycle regulation, proliferation, and apoptosis, underscoring their potential as therapeutic targets.

TOP2A + Macro and CD8+ Tex involved in immunosuppressive TME in GBC

To clarify the TIME throughout the progression of the NAT–HGIN–GBC sequence, we conducted a comprehensive subtype analysis of macrophages and T/NK cells.

Tumor-associated macrophages (TAMs) play a pivotal role in modulating immune responses and facilitating cancer progression.^[15,23] Our analysis identified eight

distinct macrophage (Macro) subpopulations, which were visualized using Uniform Manifold Approximation and Projection (UMAP) embeddings. These subpopulations were classified according to specific markers as follows: Macro1 (TOP2A+ Macro), Macro2 (CCSER1+ Macro), Macro3 (EREG+ Macro), Macro4 (FMNL2+ Macro), Macro5 (FYN+ Macro), Macro6 (IGKC+ Macro), and Macro7 (IGFBP7+ Macro) (Figures 4A, B and Supplemental Figures S4A–C, <http://links.lww.com/HC9/B964>). The analysis of cell proportions among Macro subtypes demonstrated considerable inter-group heterogeneity. Specifically, the proportion of TOP2A+ Macro cells increased progressively along the NAT–HGIN–GBC sequence, exhibiting statistical significance. These TOP2A+ Macro cells were identified as TAM cells (Figures 4C, D and Supplemental Figure S4D, <http://links.lww.com/HC9/B964>). GSEA further revealed distinct biological functions among the Macro subtypes. Notably, the TOP2A+ Macro subtype showed specific enrichment in pathways related to cell cycle regulation and DNA replication, indicating its potential role in facilitating tumor proliferation (Figure 4E). Pseudotime trajectory analysis showed that the Macro subtypes exhibited a bifurcated structure, with TOP2A+ Macro subtypes predominantly situated at the terminal stages of cellular differentiation (Figure 4F). This observation implies their participation in the concluding phases of macrophage maturation and their potential contribution to tumor progression. Furthermore, BayesPrism deconvolution analysis showed an association between the TOP2A+ Macro subtype and reduced patient survival (Figure 4G).

The identified T/NK cell populations encompass the following subtypes: CD4+ regulatory T cells (CD4+ Treg), CD4+ naïve T cells (CD4+ Tn), CD4+ memory T cells (CD4+ Tm), CD4+ exhausted T cells (CD4+ Tex), CD8+ effector T cells (CD8+ Te(1) and Te(2)), CD8+ memory T cells (CD8+ Tm(1) and Tm(2)), CD8+ exhausted T cells (CD8+ Tex), double-positive T cells (CD8+CD4+ T), and natural killer cells (NK) (Figures 5A, B and Supplemental Figure S5A, B, <http://links.lww.com/HC9/B964>). Notably, among these, only the proportion of CD8+ Tex cells exhibited a significant increase throughout the NAT–HGIN–GBC progression (Figures 5C, D and Supplemental Figure S5C, <http://links.lww.com/HC9/B964>). The CD8+ Tex subtype was found to be enriched in pathways associated with the regulation of immune responses and the functional roles of immune cells (Figure 5E). Pseudotime trajectory analysis of CD8+ T cells indicated that CD8+ Te cells act as the initial differentiated cells, CD8+ Tm cells represent an intermediate state, and these ultimately differentiate into CD8+ Tex cells (Figure 5F). Notably, the increased presence of CD8+ Tex cells was significantly correlated with poor patient survival, suggesting a potential role in the progression of GBC (Figure 5G).

Cell-type deconvolution of bulk RNA-seq data from the GSE244807 cohort demonstrated a significant positive

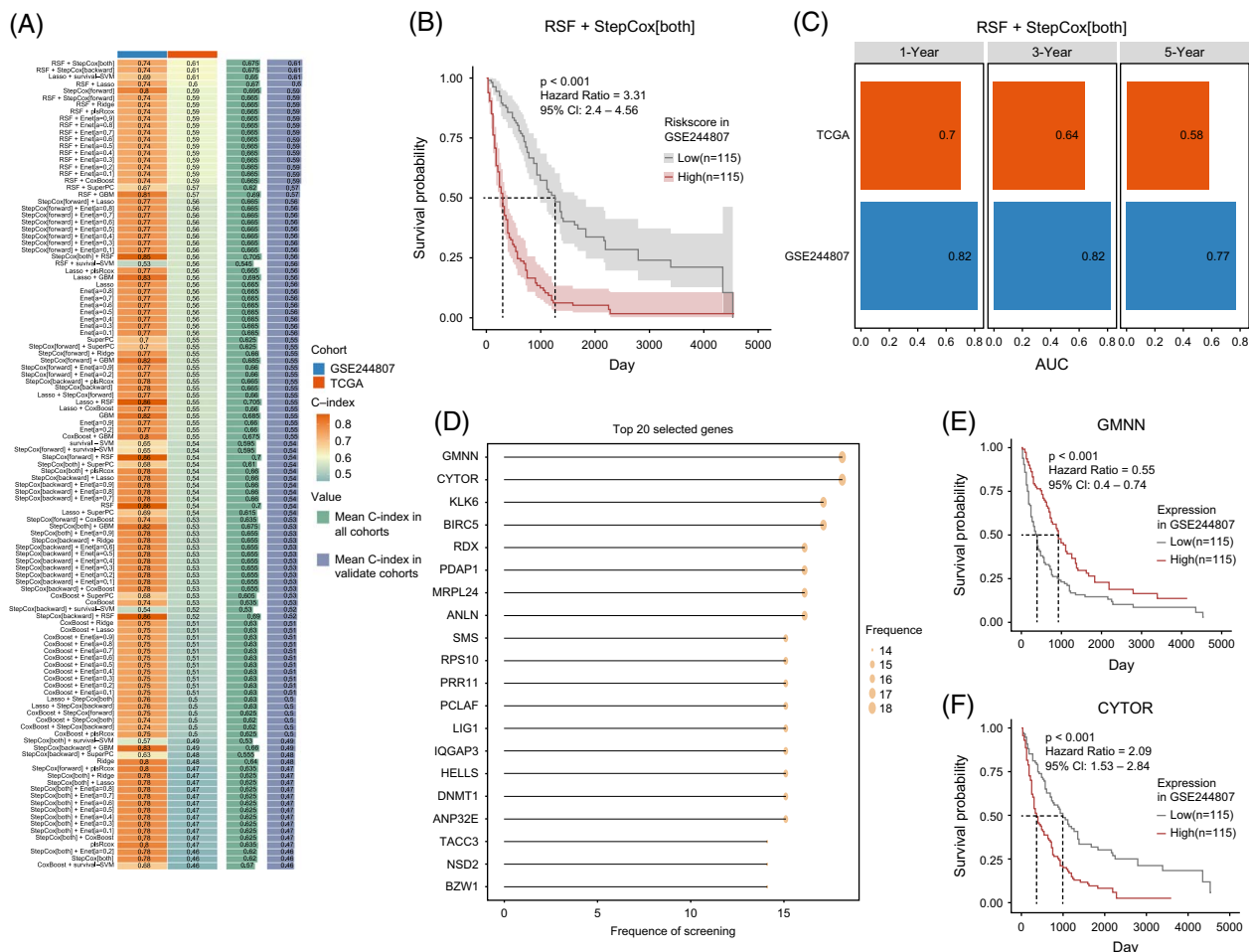


FIGURE 3 Identification and validation of prognostic gene signatures in GBC using machine learning models. (A) C-index Heatmap for Machine Learning Models: Heatmap showing the C-index values of various machine learning models across the GSE244807 and TCGA cohorts. (B) Kaplan–Meier curve illustrating survival probabilities for patients stratified into high-risk and low-risk groups based on the RSF + StepCox[both] model in the GSE244807 cohort. (C) Bar plot showing the AUC values for 1-year, 3-year, and 5-year survival predictions in the GSE244807 and TCGA cohorts on the RSF + StepCox[both] model. (D) Dot plot listing the top 20 genes as key prognostic markers. (E) Survival curve stratified by high and low expression levels of GMNN in the GSE244807 cohort. (F) Survival curve stratified by high and low expression levels of CYTOR in the GSE244807 cohort. Abbreviations: C-index, concordance index; RSF, random survival forest; StepCox, stepwise Cox regression; TCGA, The Cancer Genome Atlas.

correlation between TOP2A+ Macro and CD8+ Tex, while revealing a negative correlation with CD8+ Te, further validating the immunosuppressive role of TOP2A+ Macro (Figures 5H–J).

To explore the interactions between macrophages and T cells, we employed the CellChat R package. Our analysis revealed that TOP2A+ Macro exhibited robust interactions with other cell types, both in terms of frequency and intensity (Supplemental Figure S6A, <http://links.lww.com/HC9/B964>). Importantly, we identified that the PD-L1 signaling pathway specifically originates from TOP2A+ Macro and CD8+ Tex cells (Supplemental Figures S6B, C, <http://links.lww.com/HC9/B964>). The ligand–receptor pair involved in this pathway is CD274–PDCD1, with CD274 predominantly expressed in TOP2A+ Macro, while PDCD1 is exclusively expressed in CD8+ Tex cells (Supplemental Figure S6D, <http://links.lww.com/HC9/B964>).

In conclusion, relative to NAT and HG1N, GBC displays a markedly more pronounced immunosuppressive TME, with TOP2A + Macro and CD8+ Tex identified as pivotal subtypes contributing to this phenomenon.

TOP2A+ Epi interacts with TOP2A+ Macro and CD8+ Tex via TWEAK/FN14 signals to promote GBC

To explore the interactions between epithelial cells and TIME cells, specifically TOP2A+ Macro and CD8+ Tex, we conducted intercellular crosstalk analyses utilizing ligand–receptor pair interactions.

The analysis revealed that TOP2A+ Epi cells engage in the most extensive communication with other cell types, both in terms of the quantity and intensity of

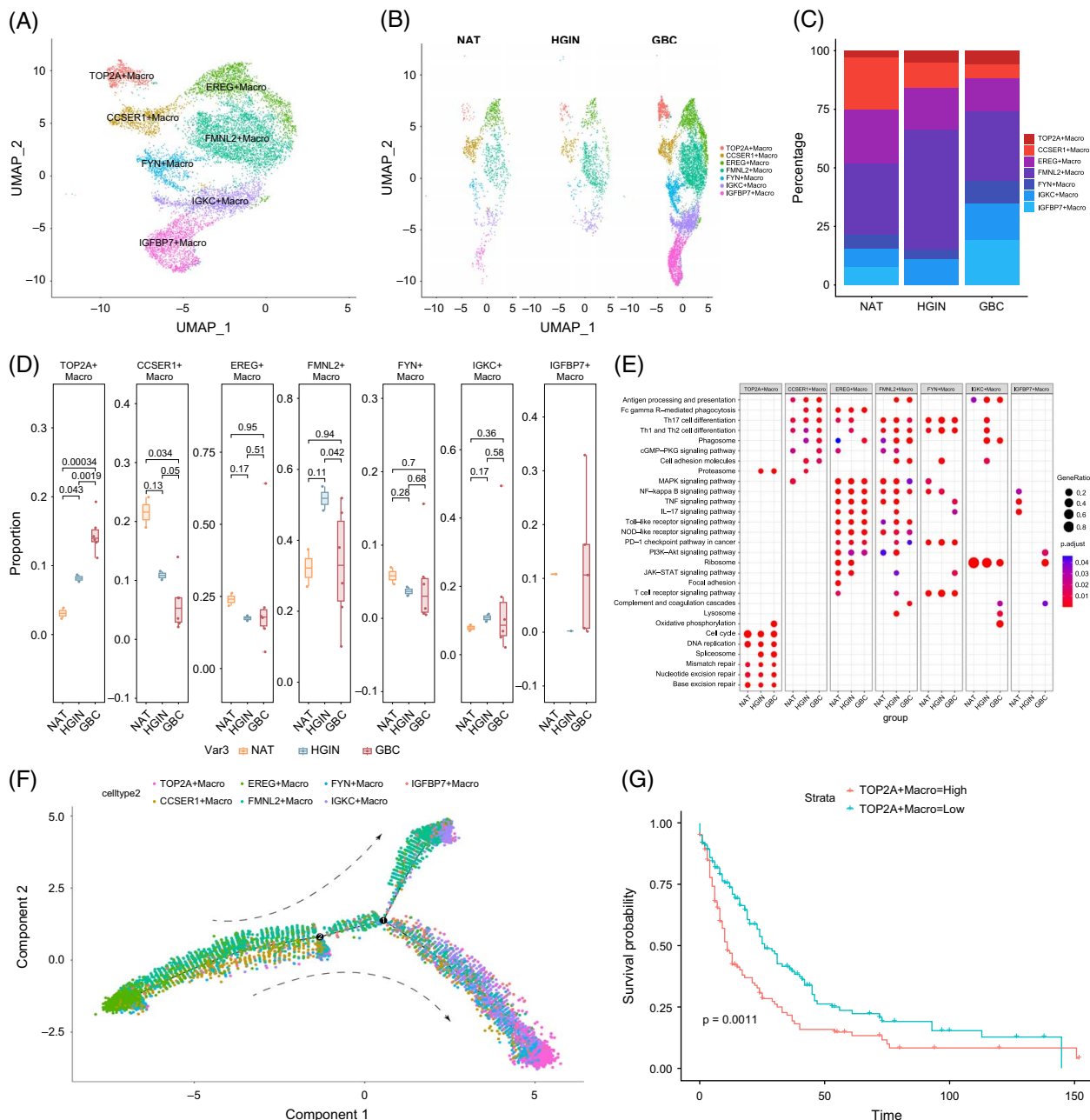


FIGURE 4 Analysis of macrophage subtypes and their role in the progression of NAT, HGIN, and GBC samples. (A) UMAP plot of macrophage subtypes showing distinct clusters. (B) UMAP plot illustrating the distribution of macrophage subtypes across groups. (C) Stacked bar plot of macrophage subtype proportions displaying the relative distribution of each subtype across groups. (D) Box plots of macrophage subtype proportions comparing the distribution of each macrophage subtype across groups, with statistical significance indicated for differences between groups. (E) Pathway enrichment dot plot showing enriched signaling pathways and biological processes in each macrophage subtype. (F) Pseudotime trajectory analysis of macrophage subtypes illustrating differentiation pathways, with arrows indicating progression direction and colors representing distinct subtypes. (G) Kaplan–Meier survival curves for patients with high and low proportions of TOP2A+ macrophages. Abbreviations: GBC, gallbladder cancer; HGIN, high-grade intraepithelial neoplasia; Macro, macrophage subtype; NAT, normal adjacent tissue; UMAP, uniform manifold approximation and projection.

interactions (Figure 6A). We identified 84 signaling pathways across eight distinct cell groups, examining their outgoing (sender) and incoming (receiver) communication patterns to elucidate intercellular signaling dynamics (Supplemental Figure S6E, <http://links.lww.com/HC9/B964>). Notably, among these pathways, the TWEAK signaling pathway was predominantly

derived from TOP2A+ Macro and TOP2A+ Epi cells (Figures 6B, C). The ligand–receptor pair was TWEAK (TNFSF12)–FN14 (TNFRSF12A), with TWEAK being primarily expressed in TOP2A+ Macro cells, whereas FN14 was predominantly expressed in TOP2A+ Epi cells (Figures 6D–F). Given the elevated specific expression of TOP2A in these two cell subtypes, we

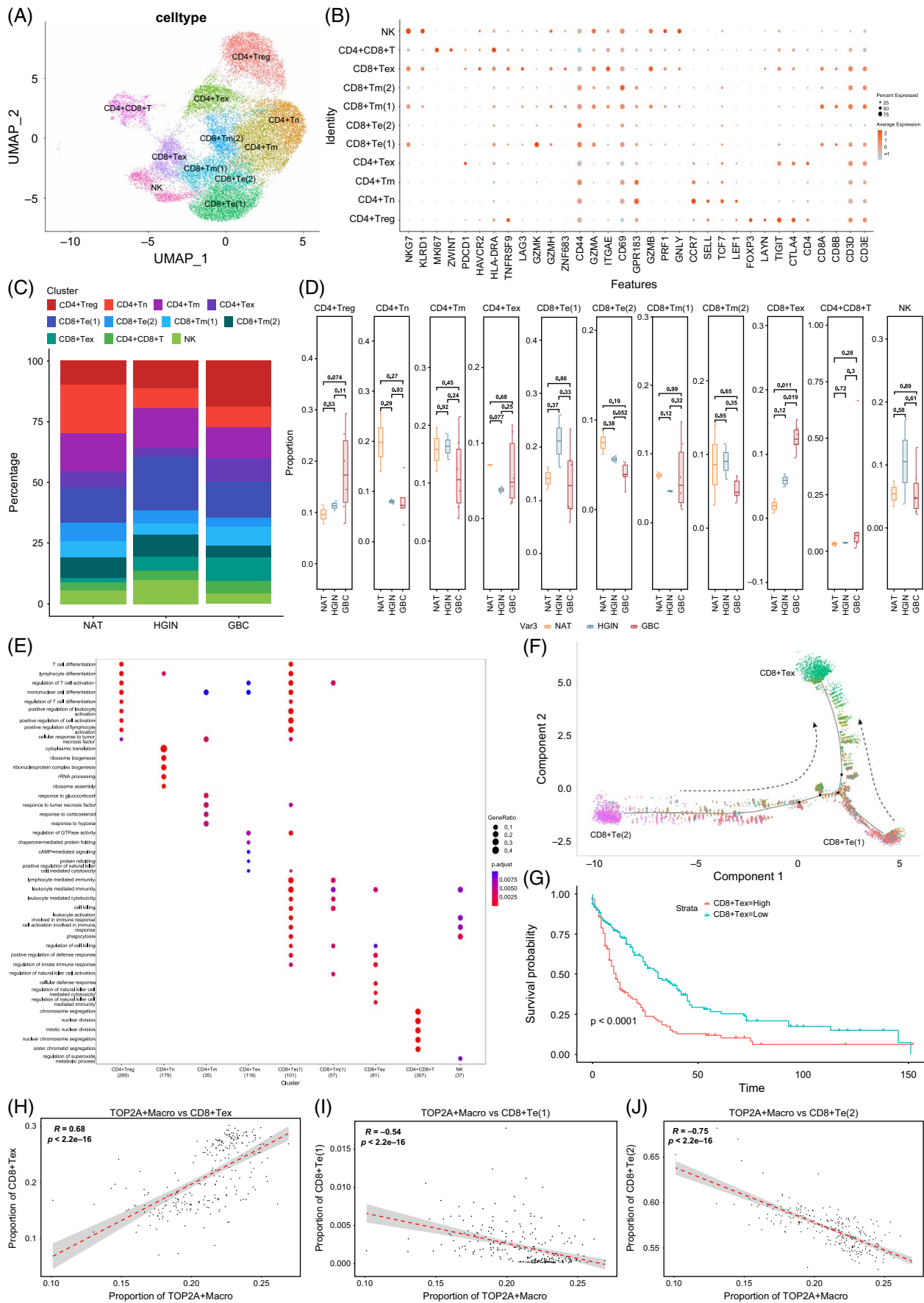


FIGURE 5 Analysis of T/NK cell subtypes. (A) UMAP plot of T cell subtypes. (B) Dot plot displaying expression levels of key marker genes across T cell subtypes. (C) Stacked bar plot of T cell subtype proportions showing the relative distribution of each subtype across groups. (D) Box plots comparing the proportions of each T cell subtype across groups. (E) Pathway enrichment dot plot showing enriched signaling pathways and biological processes in each T cell subtype. (F) Pseudotime trajectory analysis of CD8⁺ T cell subtypes showing differentiation pathways. (G) Kaplan–Meier survival curves for patients with high and low proportions of CD8⁺ Tex cells. (H–J) Correlation between TOP2A⁺ Macro and CD8⁺ Tex, CD8⁺ Te(1), and CD8⁺ Te(2) based on cell-type deconvolution in the GSE244807 cohort. Abbreviations: NK, natural killer cell; Te, effector T cell; Tex, exhausted T cell; Tm, memory T cell; Tn, naïve T cell; Treg, regulatory T cell; UMAP, uniform manifold approximation and projection.

conducted a correlation analysis, that demonstrated a significant proportional relationship between the subtypes across various samples (Figure 6G). This finding implies a close interaction between the two subtypes, with TOP2A potentially serving a critical regulatory function in this interaction. Furthermore, multiplex immunofluorescence staining indicated that GBC exhibited high expression levels of TWEAK, FN14, and TOP2A. The spatial proximity of TWEAK and FN14 underscores their ligand–receptor interaction. A substantial overlap was identified between FN14 and CD68, suggesting that FN14 originates from macrophages. Additionally, TOP2A exhibited overlap with both TWEAK and FN14, indicating its expression in both epithelial and macrophage cells (Figure 6H).

In the context of TOP2A⁺ Epi and CD8⁺ Tex, the specific cellular crosstalk is mediated by the PVR signaling pathway, with the PVR–TIGIT ligand–receptor pair being of particular significance. PVR is primarily expressed in TOP2A⁺ Epi cells, whereas TIGIT is predominantly expressed in CD8⁺ Tex cells (Supplemental Figures S6F–H, <http://links.lww.com/HCG9/B964>).

DISCUSSION

In this study, we used scRNA-seq to explore the cellular dynamics and TIME throughout the progression from NAT to HGIN and invasive GBC. We identified significant changes in cellular composition, including the emergence of the TOP2A⁺ Epi subtype and immunosuppressive cell populations, such as TOP2A⁺ Macro and CD8⁺ Tex cells, which are linked to poor outcomes. Crucial ligand–receptor interactions, encompassing the TWEAK, PD-L1, and TIGIT pathways, have been identified as mediators of immunosuppressive communication between epithelial and immune cells. This discovery underscores their potential as biomarkers and therapeutic targets for early intervention and enhanced treatment of GBC.

The progression of NAT–HGIN–GBC represents a complex, multistage carcinogenic process. Within NAT, gallbladder epithelial cells undergo genetic and epigenetic alterations in response to prolonged stimuli, such as chronic inflammation, leading to epithelial cell

proliferation and intraepithelial neoplasia, or further progression to HGIN.^[24] HGIN is considered a precursor stage of GBC, wherein HGIN progresses to GBC through the accumulation of additional genetic mutations, leading to aggressive tumor growth.^[25] By categorizing samples into 3 distinct groups, NAT, HGIN, and GBC, rather than the conventional binary classification of NAT and GBC, this study facilitates a more comprehensive molecular characterization of GBC progression and enhances our understanding of its pathogenesis.

The TOP2A gene, responsible for encoding topoisomerase II alpha, plays a critical role in cell division, exhibiting high expression levels during mitosis. It is essential for the proper condensation and segregation of chromosomes throughout mitotic progression.^[26–28] Numerous studies have identified an association between TOP2A and uncontrolled cell proliferation in various cancers.^[29–31] Nevertheless, research concerning the biological function of TOP2A in GBC remains sparse. It has been reported that TOP2A drives the proliferation and metastasis of GBC by activating the PI3K/AKT/mTOR signaling pathway.^[32] Moreover, TOP2A amplification has been identified in 17% of GBC, a rate significantly higher than that observed in other cancer types.^[33] Consequently, the mechanisms underlying TOP2A in GBC are insufficiently understood. The TOP2A⁺ Epi subtype identified in this study is crucial in the malignant progression of GBC. Currently, ML algorithm is increasingly employed in medical research to develop diagnostic and prognostic models based on transcriptional data for various cancers.^[34,35] In this study, we utilized an integrated ML algorithm approach to identify key genes from the DEGs of the TOP2A⁺ Epi subtype. The genes identified, such as GMNN, CYTOR, KLK6, and BIRC5, are promising therapeutic targets in GBC due to their significant involvement in cell cycle regulation, proliferation, and apoptosis.^[36–39]

TAMs, also known as immunosuppressive macrophages, play a pivotal role in cancer development and progression, thereby representing important therapeutic targets.^[40] Several studies have explored the potential mechanisms underlying the M2 polarization of TAMs in GBC. For instance, DLGAP5 has been demonstrated to enhance GBC cell migration and TAM M2

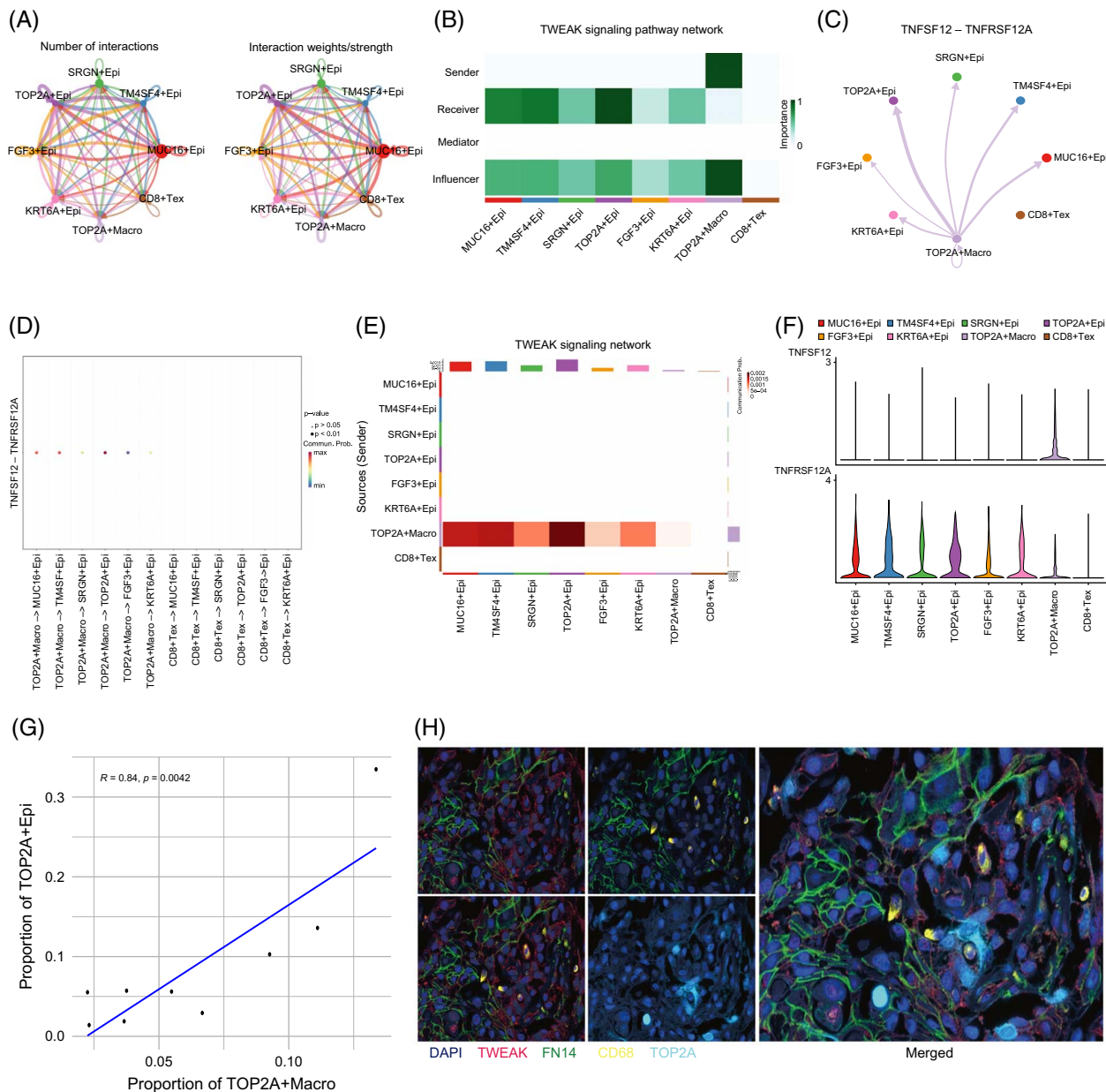


FIGURE 6 Intercellular communication analysis highlighting the TWEAK/FN14 signaling pathway between epithelial and immune cells in the GBC tumor microenvironment. (A) Intercellular communication network illustrating the number and weight/strength of interactions among cell subtypes. (B) Heatmap of the TWEAK signaling pathway network, displaying sender, receiver, mediator, and influencer roles among various cell subtypes in GBC. (C) Network diagram of the TNFSF12-TNFRSF12A (TWEAK-FN14) signaling pathway, highlighting the predominant role of TOP2A+ Macro as the ligand source and TOP2A+ Epi as the main receptor-expressing cells. (D) Dot plot visualizing ligand-receptor interactions in the TWEAK-FN14 signaling pathway across different cell subtypes. (E) Heatmap summarizing TWEAK signaling network strength across cell types. (F) Violin plots showing the expression distribution of TNFSF12 (TWEAK) and TNFRSF12A (FN14) across different cell subtypes. (G) Correlation plot demonstrating a significant positive correlation between the proportions of TOP2A+ Macro and TOP2A+ Epi cells across samples. (H) Multiplex immunofluorescence images showing the spatial distribution of TWEAK, FN14, CD68, and TOP2A. Abbreviations: CD68, cluster of differentiation 68; Epi, epithelial; FN14, fibroblast growth factor-inducible 14; Macro, macrophage; TWEAK, tumor necrosis factor-like weak inducer of apoptosis; TOP2A, topoisomerase II alpha.

polarization via activation of the cAMP signaling pathway. Similarly, nicotinamide N-methyltransferase has been shown to facilitate M2 polarization through IL-6 signaling.^[41,42] Despite these findings, the intricate crosstalk between TAMs and other cellular entities remains inadequately understood, underscoring a critical gap in our comprehension of their role in the

progression of GBC. The tumor necrosis factor-like weak inducer of apoptosis (TWEAK) engages with its exclusive receptor, fibroblast growth factor-inducible 14 (Fn14), to initiate a variety of signaling pathways, thereby contributing to multiple aspects of tumor progression.^[43] The TWEAK/Fn14 signaling axis facilitates cellular migration by activating TNF receptor-

associated factors (such as TRAF) and members of the Rho GTPase family (eg, Rac1 and Cdc42). Concurrently, it upregulates angiogenic mediators such as VEGF, thereby promoting angiogenesis.^[44,45] Furthermore, this pathway enhances the expression of pro-inflammatory cytokines (eg, TNF- α and IL-8) by activating NF- κ B signaling, thereby intensifying tumor-associated inflammation.^[46] It also drives epithelial-mesenchymal transition, which contributes to increased tumor invasiveness.^[47] Thus, the inhibition of the TWEAK/Fn14 pathway is regarded as a potential antitumor strategy, with pharmacological agents targeting this axis showing promising outcomes in both preclinical and clinical studies.^[48] The role of this pathway in GBC has not yet been documented. Our research identified that TOP2A+ Macro exhibits an increased expression of TWEAK, which interacts with its receptor Fn14 on TOP2A+ Epi, thereby eliciting tumor immune resistance in GBCs. Interestingly, both cell subtypes exhibit specific high expression levels of the TOP2A gene and display a strong correlation with each other, suggesting that TOP2A may play a regulatory role in the TWEAK-Fn14 pathway.

TOP2A+ Macro also engages in communication with CD8+ Tex cells via the PD-L1/PD-1 signaling pathway, with CD274 (PD-1) expressed in TOP2A+ macrophages and PDCD1 (PD-L1) in CD8+ exhausted T cells. The inhibition of the PD-L1/PD-1 signaling pathway through antibody blockade reactivates exhausted immune cells within the TME, thereby promoting the elimination of cancer cells.^[49] To date, various monoclonal antibodies have yielded promising results in cancer therapy. Nonetheless, the response rates of anti-PD-L1 therapies have been in several solid tumors.^[50] The application of single-cell technologies enables an in-depth exploration of the mechanisms underlying the PD-L1/PD-1 signaling pathway at a single-cell resolution, offering valuable insights for the development of more precise cell-targeted therapies.

Despite the comprehensive nature of our single-cell analysis, this study has certain limitations. First, the sample size is relatively limited, comprising only 10 patients, which may constrain the generalizability of our findings. Moreover, the infrequency of GBC and the challenges in obtaining high-quality fresh tissue samples restricted the diversity of clinical cases included in the study. Furthermore, although scRNA-seq provides valuable insights into cellular heterogeneity, it does not adequately capture the spatial relationships and interactions present within the native TME. Finally, while machine learning models have been employed to identify prognostic markers, validation in larger, independent cohorts is essential to substantiate their clinical utility. Future research should aim to overcome these limitations by increasing sample sizes, incorporating spatial transcriptomics, and undertaking additional validation analyses.

CONCLUSIONS

This study elucidates significant alterations in cellular ecosystems and intercellular signaling within the tumor TIME across the NAT-HGIN-GBC sequence, identifying TOP2A/TWEAK/FN14 as potential therapeutic targets for early intervention and enhanced patient management.

DATA AVAILABILITY STATEMENT

The raw sequence data reported in this paper have been deposited in the Genome Sequence Archive (Genomics, Proteomics & Bioinformatics 2021) in National Genomics Data Center (Nucleic Acids Res 2024), China National Center for Bioinformation/Beijing Institute of Genomics, Chinese Academy of Sciences (GSA-Human: HRA009656) that are publicly accessible at <https://ngdc.cncb.ac.cn/gsa-human>.

FUNDING INFORMATION

This research was supported by the National Natural Science Foundation of China (82072674), the Natural Science Foundation of Shandong Province (ZR2020MH258), and the Special Research Fund of Shandong Medical Association (YXH2022ZX02114).

CONFLICTS OF INTEREST

The authors have no conflicts to report.

ETHICS APPROVAL AND CONSENT TO PARTICIPATE

The study was approved by the Institutional Review Board of Qilu Hospital (registration number: KYLL-2024 (ZM)-685). Due to the retrospective nature of the study, the requirement for written informed consent was obtained from each patient. All study methods were conducted in accordance with the ethical principles outlined in the Declaration of Helsinki.

ORCID

Zhaobin He  <https://orcid.org/0000-0002-0917-0570>

Cheng Peng  <https://orcid.org/0000-0003-1217-9645>

REFERENCES

1. Roa JC, Garcia P, Kapoor VK, Maithel SK, Javle M, Koshiol J. Gallbladder cancer. *Nat Rev Dis Primers*. 2022;8:69.
2. Song X, Hu Y, Li Y, Shao R, Liu F, Liu Y. Overview of current targeted therapy in gallbladder cancer. *Signal Transduct Target Ther*. 2020;5:230.
3. Lazcano-Ponce EC, Miquel JF, Munoz N, Herrero R, Ferrecio C, Wistuba II, et al. Epidemiology and molecular pathology of gallbladder cancer. *CA Cancer J Clin*. 2001;51:349–64.
4. Sasatomi E, Tokunaga O, Miyazaki K. Precancerous conditions of gallbladder carcinoma: Overview of histopathologic characteristics and molecular genetic findings. *J Hepatobiliary Pancreat Surg*. 2000;7:556–67.
5. Kamisawa T, Kuruma S, Tabata T, Chiba K, Iwasaki S, Koizumi S, et al. Pancreaticobiliary maljunction and biliary cancer. *J Gastroenterol*. 2015;50:273–9.

6. Masuhara S, Kasuya K, Aoki T, Yoshimatsu A, Tsuchida A, Koyanagi Y. Relation between K-ras codon 12 mutation and p53 protein overexpression in gallbladder cancer and biliary ductal epithelia in patients with pancreaticobiliary maljunction. *J Hepatobiliary Pancreat Surg.* 2000;7:198–205.
7. Wistuba II, Gazdar AF, Roa I, Albores-Saavedra J. p53 protein overexpression in gallbladder carcinoma and its precursor lesions: An immunohistochemical study. *Hum Pathol.* 1996;27:360–5.
8. Wistuba II, Gazdar AF. Gallbladder cancer: Lessons from a rare tumour. *Nat Rev Cancer.* 2004;4:695–706.
9. Liu X, Zhao S, Wang K, Zhou L, Jiang M, Gao Y, et al. Spatial transcriptomics analysis of esophageal squamous precancerous lesions and their progression to esophageal cancer. *Nat Commun.* 2023;14:4779.
10. Hinshaw DC, Shevde LA. The tumor microenvironment innately modulates cancer progression. *Cancer Res.* 2019;79:4557–66.
11. Kelley RK, Ueno M, Yoo C, Finn RS, Furuse J, Ren Z, et al. Pembrolizumab in combination with gemcitabine and cisplatin compared with gemcitabine and cisplatin alone for patients with advanced biliary tract cancer (KEYNOTE-966): A randomised, double-blind, placebo-controlled, phase 3 trial. *Lancet.* 2023;401:1853–65.
12. Ren X, Zhang L, Zhang Y, Li Z, Siemers N, Zhang Z. Insights gained from single-cell analysis of immune cells in the tumor microenvironment. *Annu Rev Immunol.* 2021;39:583–609.
13. Albores-Saavedra J, de Jesus Manrique J, Angeles-Angeles A, Henson DE. Carcinoma in situ of the gallbladder. A clinicopathologic study of 18 cases. *Am J Surg Pathol.* 1984;8:323–33.
14. Zhang Y, Zuo C, Liu L, Hu Y, Yang B, Qiu S, et al. Single-cell RNA-sequencing atlas reveals an MDK-dependent immunosuppressive environment in ErbB pathway-mutated gallbladder cancer. *J Hepatol.* 2021;75:1128–41.
15. Wang X, Liu C, Chen J, Chen L, Ren X, Hou M, et al. Single-cell dissection of remodeled inflammatory ecosystem in primary and metastatic gallbladder carcinoma. *Cell Discov.* 2022;8:101.
16. Xie L, Ning Z, Hua Y, Wang P, Meng Z. Single-cell transcriptome analysis revealed the immune profile of PD-1 blockade in gallbladder carcinoma liver metastasis. *Hepatol Commun.* 2023;7:e0131.
17. Chen P, Wang Y, Li J, Bo X, Wang J, Nan L, et al. Diversity and intratumoral heterogeneity in human gallbladder cancer progression revealed by single-cell RNA sequencing. *Clin Transl Med.* 2021;11:e462.
18. He H, Chen S, Yu Y, Fan Z, Qian Y, Dong Y, et al. Comprehensive single-cell analysis deciphered microenvironmental dynamics and immune regulator olfactomedin 4 in pathogenesis of gallbladder cancer. *Gut.* 2024;73:1529–42.
19. Gulati GS, Sikandar SS, Wesche DJ, Manjunath A, Bharadwaj A, Berger MJ, et al. Single-cell transcriptional diversity is a hallmark of developmental potential. *Science.* 2020;367:405–11.
20. Zhang L, Li Z, Skrzypczynska KM, Fang Q, Zhang W, O'Brien SA, et al. Single-cell analyses inform mechanisms of myeloid-targeted therapies in colon cancer. *Cell.* 2020;181:442–459.e29.
21. Liu H, Zhang W, Zhang Y, Adegboro AA, Fasoranti DO, Dai L, et al. Mime: A flexible machine-learning framework to construct and visualize models for clinical characteristics prediction and feature selection. *Comput Struct Biotechnol J.* 2024;23:2798–810.
22. Jin S, Guerrero-Juarez CF, Zhang L, Chang I, Ramos R, Kuan CH, et al. Inference and analysis of cell–cell communication using CellChat. *Nat Commun.* 2021;12:1088.
23. Cheng S, Li Z, Gao R, Xing B, Gao Y, Yang Y, et al. A pancreatic single-cell transcriptional atlas of tumor infiltrating myeloid cells. *Cell.* 2021;184:792–809.e23.
24. Sturm N, Schuhbaur JS, Hüttner F, Perkhof L, Ettrich TJ. Gallbladder cancer: Current multimodality treatment concepts and future directions. *Cancers.* 2022;14:5580.
25. Nakanuma Y, Sugino T, Nomura Y, Watanabe H, Terada T, Sato Y, et al. Association of precursors with invasive adenocarcinoma of the gallbladder: A clinicopathological study. *Ann Diagn Pathol.* 2022;58:151911.
26. Thakurela S, Garding A, Jung J, Schübeler D, Burger L, Tiwari VK. Gene regulation and priming by topoisomerase II α in embryonic stem cells. *Nat Commun.* 2013;4:2478.
27. Ali Y, Abd Hamid S. Human topoisomerase II alpha as a prognostic biomarker in cancer chemotherapy. *Tumour Biol.* 2016;37:47–55.
28. Uusküla-Reimand L, Wilson MD. Untangling the roles of TOP2A and TOP2B in transcription and cancer. *Sci Adv.* 2022;8:eadd4920.
29. Zhang R, Xu J, Zhao J, Bai JH. Proliferation and invasion of colon cancer cells are suppressed by knockdown of TOP2A. *J Cell Biochem.* 2018;119:7256–63.
30. Pei YF, Yin XM, Liu XQ. TOP2A induces malignant character of pancreatic cancer through activating β -catenin signaling pathway. *Biochim Biophys Acta Mol Basis Dis.* 2018;1864:197–207.
31. Wang K, Jiang X, Jiang Y, Liu J, Du Y, Zhang Z, et al. EZH2-H3K27me3-mediated silencing of mir-139-5p inhibits cellular senescence in hepatocellular carcinoma by activating TOP2A. *J Exp Clin Cancer Res.* 2023;42:320.
32. Lyu WJ, Shu YJ, Liu YB, Dong P. Topoisomerase II alpha promotes gallbladder cancer proliferation and metastasis through activating phosphatidylinositol 3-kinase/protein kinase B/mammalian target of rapamycin signaling pathway. *Chin Med J.* 2020;133:2321–9.
33. Heestand GM, Schwaederle M, Gatalica Z, Arguello D, Kurzrock R. Topoisomerase expression and amplification in solid tumours: Analysis of 24,262 patients. *Eur J Cancer.* 2017;83:80–7.
34. Liu Z, Liu L, Weng S, Guo C, Dang Q, Xu H, et al. Machine learning-based integration develops an immune-derived lncRNA signature for improving outcomes in colorectal cancer. *Nat Commun.* 2022;13:816.
35. Zhang W, Dang R, Liu H, Dai L, Liu H, Adegboro AA, et al. Machine learning-based investigation of regulated cell death for predicting prognosis and immunotherapy response in glioma patients. *Sci Rep.* 2024;14:4173.
36. Zhao X, Zhang X, Shao S, Yang Q, Shen C, Yang X, et al. High expression of GMNN predicts malignant progression and poor prognosis in ACC. *Eur J Med Res.* 2022;27:301.
37. Wang W, Yun B, Hoyle RG, Ma Z, Zaman SU, Xiong G, et al. CYTOR facilitates formation of FOSL1 phase separation and super enhancers to drive metastasis of tumor budding cells in head and neck squamous cell carcinoma. *Adv Sci.* 2024;11:e2305002.
38. Hwang YS, Cho HJ, Park ES, Lim J, Yoon HR, Kim JT, et al. KLK6/PAR1 axis promotes tumor growth and metastasis by regulating cross-talk between tumor cells and macrophages. *Cells.* 2022;11:4101.
39. Frazzi R. BIRC3 and BIRC5: Multi-faceted inhibitors in cancer. *Cell Biosci.* 2021;11:8.
40. Noy R, Pollard JW. Tumor-associated macrophages: From mechanisms to therapy. *Immunity.* 2014;41:49–61.
41. Huang J, Zheng M, Li Y, Xu D, Tian D. DLGAP5 promotes gallbladder cancer migration and tumor-associated macrophage M2 polarization by activating cAMP. *Cancer Immunol Immunother.* 2023;72:3203–16.
42. Li Y, Yang B, Miao H, Liu L, Wang Z, Jiang C, et al. Nicotinamide N-methyltransferase promotes M2 macrophage polarization by IL6 and MDSC conversion by GM-CSF in gallbladder carcinoma. *Hepatology.* 2023;78:1352–67.
43. Hu G, Zeng W, Xia Y. TWEAK/Fn14 signaling in tumors. *Tumour Biol.* 2017;39:1010428317714624.
44. Vince JE, Chau D, Callus B, Wong WWL, Hawkins CJ, Schneider P, et al. TWEAK–FN14 signaling induces lysosomal

- degradation of a cIAP1–TRAF2 complex to sensitize tumor cells to TNF α . *J Cell Biol.* 2008;182:171–84.
45. Fortin SP, Ennis MJ, Schumacher CA, Zylstra-Diegel CR, Williams BO, Ross JTD, et al. Cdc42 and the guanine nucleotide exchange factors Ect2 and trio mediate Fn14-induced migration and invasion of glioblastoma cells. *Mol Cancer Res.* 2012;10:958–68.
46. Winkles JA, Tran NL, Brown SA, Stains N, Cunliffe HE, Berens ME. Role of TWEAK and Fn14 in tumor biology. *Front Biosci.* 2007;12:2761–71.
47. Michaelson JS, Cho S, Browning B, Zheng TS, Lincecum JM, Wang MZ, et al. Tweak induces mammary epithelial branching morphogenesis. *Oncogene.* 2005;24:2613–24.
48. Cheng E, Armstrong CL, Galisteo R, Winkles JA. TWEAK/Fn14 axis-targeted therapeutics: Moving basic science discoveries to the clinic. *Front Immunol.* 2013;4:473.
49. Cha JH, Chan LC, Li CW, Hsu JL, Hung MC. Mechanisms controlling PD-L1 expression in cancer. *Mol Cell.* 2019;76:359–70.
50. Gong J, Chehraz-Raffle A, Reddi S, Salgia R. Development of PD-1 and PD-L1 inhibitors as a form of cancer immunotherapy: A comprehensive review of registration trials and future considerations. *J Immunother Cancer.* 2018;6:8.

How to cite this article: He Z, Cao J, Wang X, Yang S, Gao H, Yu Y, et al. Single-cell analyses unravel ecosystem dynamics and intercellular crosstalk during gallbladder cancer malignant transformation. *Hepatol Commun.* 2025;9:e0697. <https://doi.org/10.1097/HC9.0000000000000697>